EDU Journal of Computer and Electrical Engineering

Journal home page : www.edu-journals.com

Effects of Operating Temperature on the Performance of c-Si, a-Si:H, CIGS, and CdTe/CdS Based Solar Cells

Ahnaf Shahriar[1]✉, Saif Hasnath[1], Md. Aminul Islam[1]✉

[1]*School of Science Engineering and Technology, East Delta University, Abdullah Al Noman Road, Noman Society, East Nasirabad, Khulshi, Chattogram 4209, Bangladesh*

Received: September 25, 2020
Revised: October 25, 2020
Accepted: April 11, 2021

Keywords
Solar Cell
SCAPS-1D
IV Characteristics
Temperature Coefficient
Quantum Efficiency

Abstract: Solar photovoltaic technology is one of the most promising, economical and green technologies to harvest energy with the least effect on the environment. Crystalline silicon (c-Si), amorphous silicon (a-Si), CIGS, CdTe/CdS etc., are dominating the PV market. Operating temperature plays an important role in the performance of solar cells. A comparative investigation on the effect of operating temperature on the market available solar cells is very important in choosing the better PV technology in high-temperature applications. In this study, the performances of different solar cell technologies, namely crystalline silicon (c-Si), amorphous silicon (a-Si), CIGS, and CdTe/CdS based solar cells, have been investigated under different operating temperature by using SCAPS-1D simulation software. All parameter of a solar cell for different technology has been studied under the varying operation temperature ranging from 25 °C to 70 °C and the rate of change of them has been recorded. It has been found that the Voc and Pmax degrade significantly and Isc increases slightly with an increase in temperature. The temperature coefficients of Pmax for c-Si, a-Si, CdTe and CIGS have been found as -0.0724/K, -0.0362/K, -0.0112/K and -0.0663/K, respectively. On the other hand, c-Si and CIGS technologies show better quantum efficiency behaviour in both room and high operating temperatures.

1. INTRODUCTION

Installation capacity and demand for solar photovoltaic (PV) technology are gradually increasing over the world. It is estimated that by the year 2024, photovoltaic solar cells will be producing 1.5TW of electrical energy [1]. Among the different PV cell technologies, crystalline silicon (c-Si), hydrogenated amorphous silicon (a-Si:H), cadmium telluride (CdTe), and copper indium gallium di-selenide (CIGS) solar cells are mostly used in real field application [2]. Solar PV module performances are affected by different real field operating conditions such as solar radiation [3], temperature [4], dust deposition [5],[6] humidity [7], rain [8], etc. Among these operating conditions, solar irradiation and cell temperature fluctuate rapidly with time, and PV module performance also fluctuated [9]-[11]. Hishikawa et al. [12] reported the effect of temperature on the performance of crystalline silicon PV cell where V_{oc} decreases with a maximum 0.35%/°C. Temperature-dependent performance CdTe solar cell has been reported in [13],[14]. Anwar et al. [15]reported the negative temperature coefficient of efficiency 0.05-0.06/°C of the nw-CdTe solar cell. The temperature gradient of -0.032%/°C was reported for CIGS solar cell [16]. The temperature-dependent performance of the solar cell is very significant, especially in concentrated solar application where cell temperature reaches a very high temperature. In literature, lots of reports related to the effect of operating temperature on the performance of individual solar cells are available. However, comparative features of temperature-dependent characteristics of different solar cells are very few. So the objective of the study to investigate and compare the temperature-dependent performances of varying PV technologies to evaluate the better technology in high-temperature application. In this study, variations of electrical parameters (V_{oc}, I_{sc}, P_{max}, FF, efficiency, and quantum efficiency) of c-Si, a-Si:H, CdTe and CIGS solar cells at different operating temperatures have been compared.

✉Corresponding author. E-mail address: ahnaf.winchester@gmail.com (Ahnaf Shahriar), aminulmse@gmail.com (Md. Aminul Islam)

Available online at http://edu-journals.com/index.php/ejcee
https://doi.org/ 10.46603/ejcee.v1i1.21

2. METHODOLOGY

A comparative investigation between different PV technologies has been carried out through simulation software Scaps 1D developed at the Electronic and Information System Department, Gent University, Belgium [17]. The four common PV technologies such as c-Si, a-Si:H, CdTe, CIGS structure have been taken in this study. Figure 1 shows the structures of different solar PV cells. In this study, the traditional Poly-crystalline Silicon structure has been taken with p+ Si BSF/ p-Si Bulk/ p-Si Front/ n-Si layers. Parameters for each layer have been pre-set according to the traditional c-Silicon, as shown in Table 1. A simple p-i-n structure has been considered for hydrogenated amorphous silicon (a-Si:H) solar cell. The considered relevant parameters have been shown in Table 2. The structure for Cadmium Telluride (CdTe) solar cells, layers has been set as CdTe(cont)/CdTe/CdS. The relevant parameters have been set as shown in
Table 3. The layered structure for Copper-Indium-Gallium-Arsenide (CIGS) solar cell has been set as i-ZnO/CdS/OVC/CIGS. Parameters for each layer have been pre-set according to Table 4.

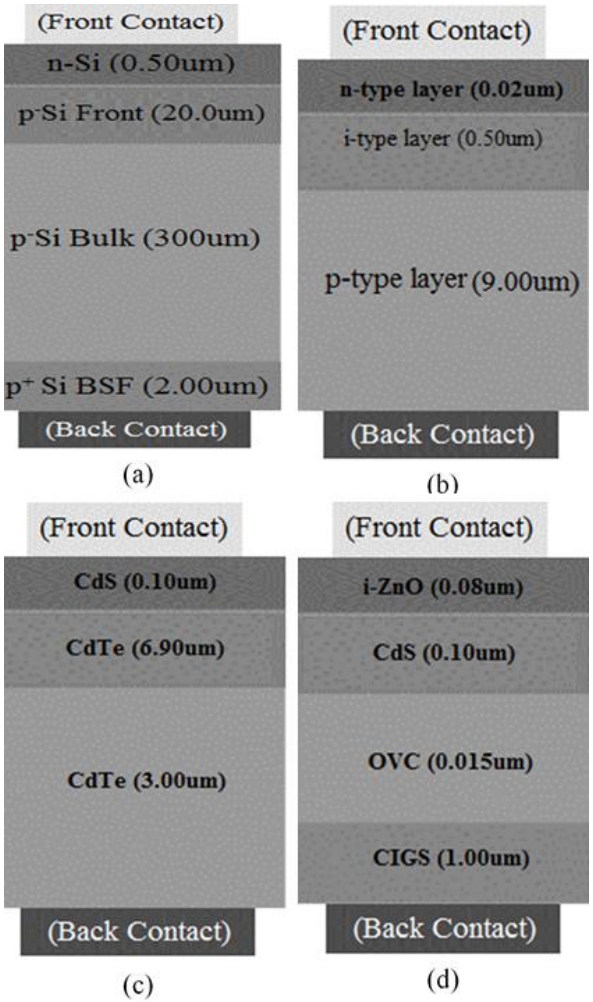

Figure 1. Solar PV cell structure of (a) Crystalline Silicon (b) Hydrogenated Amorphous Silicon cell (c) Cadmium Telluride Cell and (d) CIGS.

SCAPS can analyse the basic semiconductor equation, Poisson equation and continuity equation for both holes and electrons as shown in Equations (1-5). These are one-dimensional equations used in the evaluation of solar cell models [18-20].

$$\frac{\partial}{\partial x}(\varepsilon_o \varepsilon \frac{\partial \psi}{\partial x}) = -q(p - n + N_D^+ - N_A^- + \frac{\rho_{def}}{q} \quad (1)$$

$$-\frac{\partial J_n}{\partial x} - U_n + G = \frac{\partial n}{\partial t} \quad (2)$$

$$-\frac{\partial J_p}{\partial x} - U_p + G = \frac{\partial p}{\partial t} \quad (3)$$

$$J_n = -\frac{\mu_n n}{q}\frac{\partial E_{Fn}}{\partial x} \quad (4)$$

$$J_p = -\frac{\mu_p n}{q}\frac{\partial E_{Fp}}{\partial x} \quad (5)$$

Where, ε_o absolute permittivity ε *is* relative permittivity or dielectric constant, q is the charge of an electron, N_D^+ is the Donor concentration, N_A^- is the Acceptor concentration, μ_n is the electron mobility, μ_p is the hole mobility, J_n electron current density, J_p is hole current density, G is the rate of carrier generation, E_{Fn} quasi Fermi level of conduction band, E_{Fp} quasi Fermi level of valance band. Equations (1-3) explain the simulation of each semiconductor layers together with 4 and 5, which shows the relation of electron current density and hole current density with the corresponding quasi Fermi-level.
Figure 2 shows the flow chart of the simulation process.

Table 1. Physical parameters for Crystalline Silicon structure.

Parameters	p^+ Si BSF	p^- Si Bulk	p^- Si Front	n-Si
Thickness(μm)	2.0	300	20	0.5
Band gap (eV)	1.12	1.12	1.12	1.12
Electron affinity (eV)	4.5	4.5	4.5	4.5
Dielectric permittivity	11.9	11.9	11.9	11.9
N_c (1/cm^3)	2.8×10^{19}	2.8×10^{19}	2.8×10^{19}	2.8×10^{19}
N_v (1/cm^3)	1.04×10^{19}	1.04×10^{19}	1.04×10^{19}	1.04×10^{19}
υ_e (cm/s)	1.0×10^{7}	1.0×10^{7}	1.0×10^{7}	1.0×10^{7}
υ_h (cm/s)	1.0×10^{7}	1.0×10^{7}	1.0×10^{7}	1.0×10^{7}
μ_e (cm^2/Vs)	1.5×10^{3}	1.5×10^{3}	1.5×10^{3}	1.5×10^{3}
μ_h (cm^2/Vs)	4.5×10^{3}	4.5×10^{3}	4.5×10^{3}	4.5×10^{3}
Doping (1/cm^3)	1.0×10^{12}	1.0×10^{12}	1.0×10^{12}	1.0×10^{12}
N_d (1/cm^3)				1.0×10^{20}
N_a (1/cm^3)	1.0×10^{19}	1.0×10^{16}	1.0×10^{16}	

Table 2. Physical parameters for amorphous silicon (a-S:H) structure.

Parameters	p-layer	i-layer	n-layer
Thickness (μm)	9.0	0.5	0.02
Band gap (eV)	1.8	1.8	1.8
Electron affinity (eV)	3.9	3.9	3.9
Dielectric permittivity	11.9	11.9	11.9
N_c (1/cm^3)	1.0×10^{20}	1.0×10^{20}	1.0×10^{20}
N_v (1/cm^3)	1.0×10^{20}	1.0×10^{20}	1.0×10^{20}
υ_e (cm/s)	1.0×10^{6}	1.0×10^{6}	1.0×10^{6}
υ_h (cm/s)	1.0×10^{6}	1.0×10^{6}	1.0×10^{6}
μ_e (cm^2/Vs)	20	20	20
μ_h (cm^2/Vs)	5.0	5.0	5.0
N_d (1/cm^3)	1.0×10^{6}	1.0×10^{6}	1.0×10^{17}
N_a (1/cm^3)	1.0×10^{17}	1.0×10^{6}	1.0×10^{6}

https://dx.doi.org/10.46603/ejcee.v1i1.21

Table 3. Physical parameters for Cadmium Telluride structure.

Parameters	CdTe (cont.)	CdTe	CdS
Thickness(μm)	3	6.9	0.10
Band gap (eV)	1.45	1.45	2.45
Electron affinity (eV)	4.3	4.3	4.5
Dielectric permittivity	10	10	10
N_c (1/cm^3)	1.3×10^{18}	1.3×10^{18}	1.5×10^{18}
N_v (1/cm^3)	7.6×10^{18}	7.6×10^{18}	1.8×10^{18}
υe (cm/s)	1.0×10^{7}	1.0×10^{7}	1.0×10^{7}
υ_h (cm/s)	1.0×10^{7}	1.0×10^{7}	1.0×10^{7}
μ_e (cm^2/Vs)	50	50	50
μ_h (cm^2/Vs)	30	30	20
N_d (1/cm^3)			1.0×10^{17}
N_a (1/cm^3)	2.0×10^{14}	1.0×10^{13}	0

Table 4. Physical parameters for Copper-Indium-Gallium-Diselenide structure.

Parameters	CIGS	OVC	CDS	i-ZNO
Thickness(μm)	1.0	0.015	0.10	0.08
Bandgap (eV)	1.2	1.45	2.45	3.4
Electron affinity (eV)	4.5	4.5	4.45	4.55
Dielectric permittivity	10	10	10	10
N_c (1/cm^3)	2.0×10^{18}	2.0×10^{18}	2.0×10^{18}	4.0×10^{18}
N_v (1/cm^3)	2.0×10^{18}	2.0×10^{18}	1.5×10^{19}	9.0×10^{18}
υe (cm/s)	1.0×10^{7}	1.0×10^{7}	1.0×10^{7}	1.0×10^{7}
υ_h (cm/s)	1.0×10^{7}	1.0×10^{7}	1.0×10^{7}	1.0×10^{7}
μ_e (cm^2/Vs)	50	1.0	50	50
μ_h (cm^2/Vs)	20	1.0	20	20
Doping (1/cm^3)	1.0×10^{18}	1.0×10^{17}		
N_d (1/cm^3)		1.0×10^{13}	1.0×10^{15}	5.0×10^{17}
N_a (1/cm^3)	5.5×10^{15}			

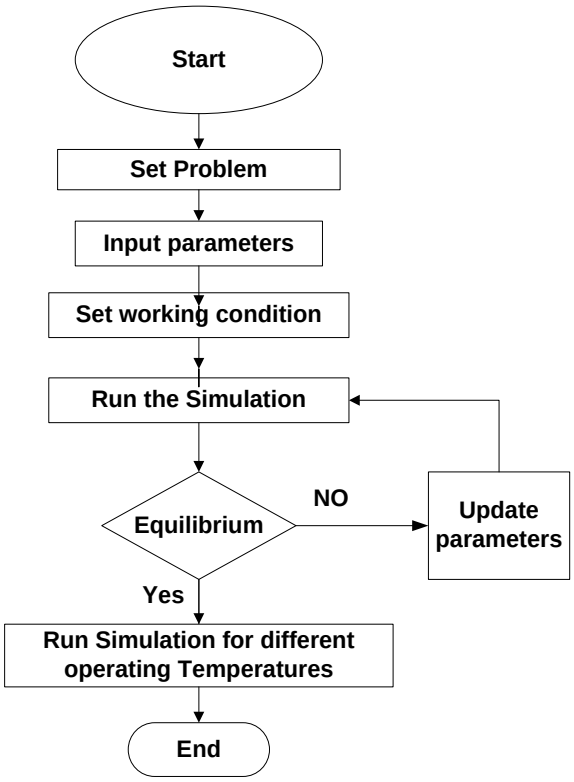

Figure 2. Flowchart of simulation methodology.

The PV solar cell parameters such as V_{oc}, I_{sc}, FF, V_{mpp}, I_{mpp} and P_{max} are determined for each cell structure under the constant Illumination of 1000W/m^2 with air mass of (AM1.5). The solar cell parameters were recorded at different operating temperatures from 300K to 360K with a step of 17° K. The final data were graphically represented against the varying temperature and temperature coefficients (TC).

3. RESULTS AND DISCUSSIONS

3.1 IV curve

The IV curves of c-Si solar cell at 1000W/m^2 and different operating temperatures are shown in Figure 3. Open circuit voltage (V_{oc}) gradually decreases with an increase in temperature. The bandgap of semiconductor decreases at higher temperature and V_{oc} is proportional to the bandgap. So that V_{oc} and V_{mp} both decrease with the increase in temperature [21]. The obtained V_{oc} values were 0.62 and 0.48 volt at 300 and 360K, respectively, as shown in Table 5. Efficiency and fill factor (FF) also decrease with the increase of temperature. The obtained efficiency drops from 18.42% to 14.04% due to temperature rise from 300K to 360K as shown in Table 5. On the other hand, the short circuit current (I_{sc}) increases slightly with increased temperature due to the increase of carrier generation and reducing bandgap at high temperature [22]. The obtained I_{sc} values at 300K and 360K are 35.1mA and 37.3mA, respectively.

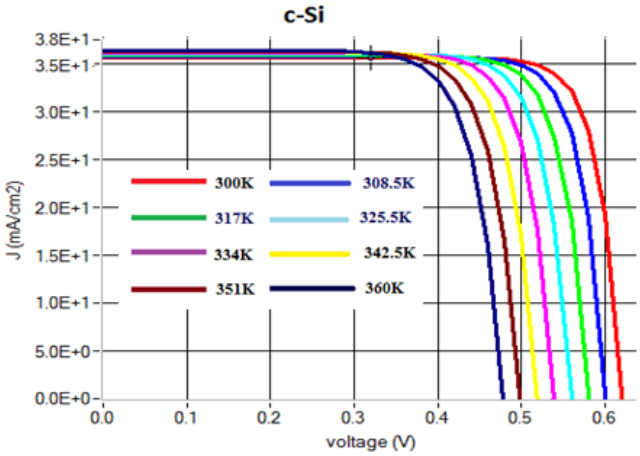

Figure 3. Effect of operating temperature on IV curve of c-Si solar cell.

The IV curves of a-Si:H solar cell at 1000W/m^2 and different operating temperatures are shown in Figure 4. Open circuit voltage (V_{oc}) gradually decreases with the increase of temperature. The bandgap of semiconductor decreases at higher temperature and V_{oc} is proportional to the bandgap. So that V_{oc} and V_{mp} both decrease with increasing the temperature [21]. The obtained V_{oc} values were 0.55 and 0.40 volt at 300 and 36,0K, respectively, as shown in Table 5. Efficiency and fill factor (FF) also decrease with increase of temperature. The obtained efficiency drops from 11.42% to 9.61% due to temperature rise from 300K to 360K, as shown in Table 5. The IV curves of CdTe solar cell at 1000W/m^2 and different operating temperatures are shown in Figure 5. Open circuit voltage (V_{oc}) gradually decreases with the increase of temperature. The bandgap of semiconductor decreases at higher temperature and V_{oc} is proportional to the bandgap. So that V_{oc} and V_{mp} both decrease with the increase in temperature [21]. The obtained V_{oc} values were 0.75 and 0.59 volt at 300 and 360K, respectively, as shown in Table 5. Efficiency

https://dx.doi.org/10.46603/ejcee.v1i1.21

and fill factor (FF) also decrease with the increase of temperature. The obtained efficiency drops from 7.33% to 6.79% as a consequence of temperature rise from 300K to 360K as shown in Table 5. On the other hand, the short circuit current (I_{sc}) increases slightly with increase of temperature due to the increase of carrier generation rate at high temperature. The obtained I_{sc} values at 300 and 360K are 21.63mA and 22.75mA, respectively.

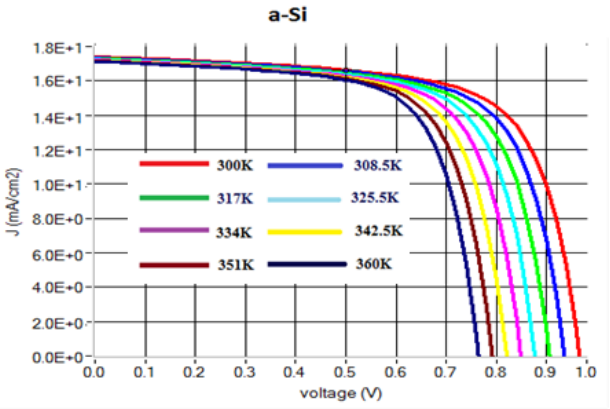

Figure 4. Effect of operating temperature on IV curve of a-Si:H solar cell.

The IV curves of CIGS solar cell at 1000W/m² and different operating temperatures are shown in Figure 6. Open circuit voltage (Voc) gradually decreases with the increase of temperature. The bandgap of semiconductor decreases at higher temperature and Voc is proportional to the bandgap. So that Voc and Vmp both decrease with the increase in temperature [21]. The obtained V_{oc} values were 0.55 and 0.40 volt at 300 and 360K, respectively as shown in Table 5. Efficiency and fill factor (FF) also decrease with increase of temperature. The obtained efficiency drops from 10.86% to 6.88% as a consequence of temperature rise from 300K to 360K as shown in Table 5. On the other hand, the short circuit current (I_{sc}) increases slightly with the increase of temperature due to the increase of carrier generation rate at high temperature. The obtained I_{sc} values at 300K and 360K are 31.681mA and 30.96mA, respectively.

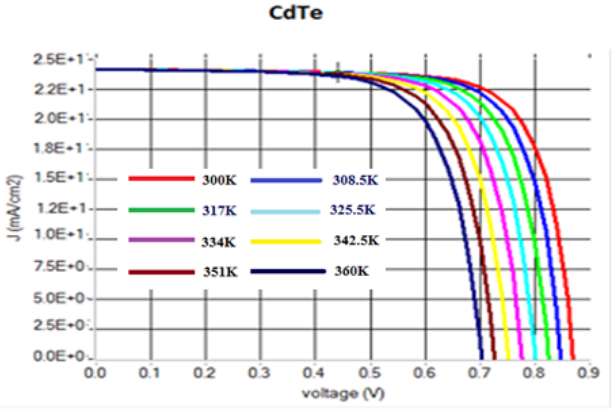

Figure 5. Effect of operating temperature on IV curve of CdTe solar cell.

3.2 Temperature coefficient

Temperature coefficients of different electrical parameters have been obtained from the temperature versus plots, as shown in Figure 7. Rate of change of V_{oc}, I_{sc}, P_{max}, and efficiency of c-Si, a-Si:H, CdTe and CIGS PV cells with increasing the operating temperature is presented in Figure 7 (a)-(d).

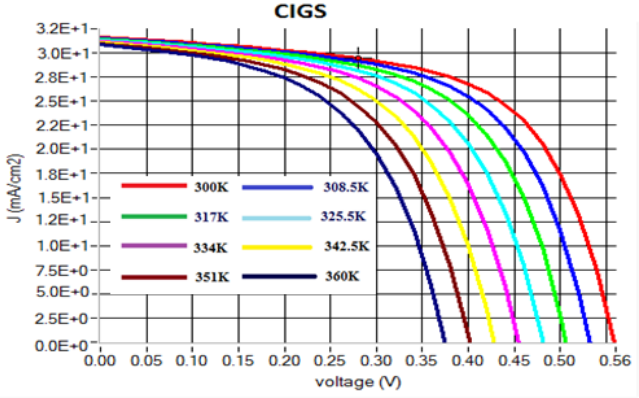

Figure 6. Effect of operating temperature on IV curve of CIGS solar cell.

The V_{oc}, P_{max}, and efficiency of all four solar cells decrease with increasing the temperature; on the other side, I_{sc} slightly increases with temperature. Over the entire temperature variation, c-Si solar cell seems to have a lower tangent value of Voc than other cells as shown in Figure 7(a), which means reducing the bandgap of c-Si with the increase of temperature was a lesser amount. CdTe cell shows the highest temperature stability in case of a reduction of P_{max} and efficiency. In considering of high-temperature application, especially at a concentrated solar application where operating temperature of a solar cell is very high, CdTe technology seems to be a better candidate. Table 6 exhibits the temperature coefficient (TC) of different light IV parameters of four solar cells. The TC of V_{oc} of c-Si, CdTe, CIGS, and a-Si were -0.0020/K ,-0.0024/K, -0.0026/K and -0.0028/K, respectively. The lowest temperature impact on V_{oc} was found for the c-Si solar cell. The TC values of P_{max} of c-Si, CdTe, CIGS, and a-Si were -0.0724/K ,-0.0112/K, -0.0663/K and -0.0362/K, respectively. The lowest temperature impact on P_{max} was found for the CdTe solar cell.

3.3 Spectral Response

Spectral responses have been compared by detecting quantum efficiency curves of different solar PV technologies. Figure 8 (a) shows the external quantum efficiency (QE) curves of c-Si, a-Si:H, CdTe and CIGS solar cells at 1000W/m² and 300K temperature. The a-Si solar cell possesses the highest QE at the blue region up to 450nm wavelength, and then QE of a-Si drops rapidly and closes to zero at 800nm range. On the other hand, above 550nm wavelength, c-Si possess higher QE characteristic. CIGS technology exhibits more or less similar QE behaviour to c-Si solar cell. CdTe shows the worst QE characteristics with a maximum efficiency of 30% at 850nm and after this QE drops to zero. At high temperature (360K), QE of all cells increases significantly due to the decrease of the band gap, as shown in Figure 8 (b). However, a comparative feature of QE characteristics at high temperature is pretty similar to the low

https://dx.doi.org/10.46603/ejcee.v1i1.21

temperature. In the blue region (300 to 550nm), a-Si possesses the highest QE, wherein the red region (550 to 900 nm), c-Si holds the highest QE. Better overall QE characteristics were found for c-Si solar cell.

Table 5. Light IV parameters values of different solar cells at 300 and 360K temperature.

	c-Si		a-Si-H		CdTe		CIGS	
Parameters	**At 300°K**	**At 360°K**	**At 300°K**	**At 360°K**	**At 300°K**	**At 360°K**	**At 300°K**	**At 360°K**
$V_{oc}(V)$	0.62	0.48	0.55	0.40	0.75	0.59	0.55	0.40
$I_{sc}(mA)$	35.1	37.3	17.39	17.15	21.63	22.75	31.68	30.96
$V_{mpp}(V)$	0.54	0.41	0.78	0.64	0.47	0.4	0.42	0.28
$I_{mpp}(mA)$	33.78	34.10	14.75	14.69	15.29	16.77	25.55	23.95
$FF(\%)$	83.02	77.48	69.15	69.33	44.79	50.11	61.80	55.29
$\eta(\%)$	18.42	14.04	11.41	9.61	7.33	6.79	10.86	6.88

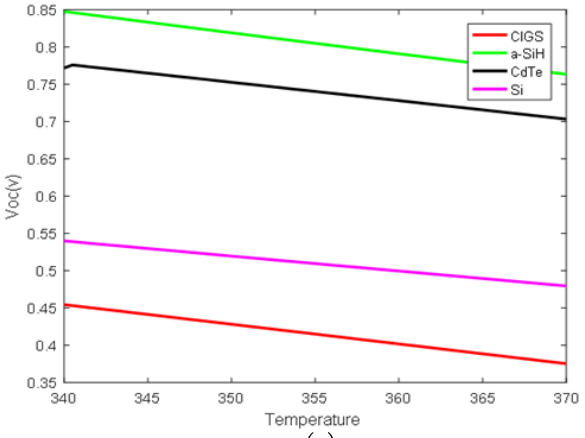

(a)

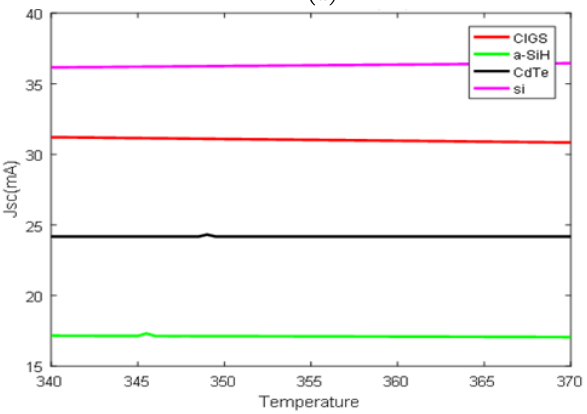

(b)

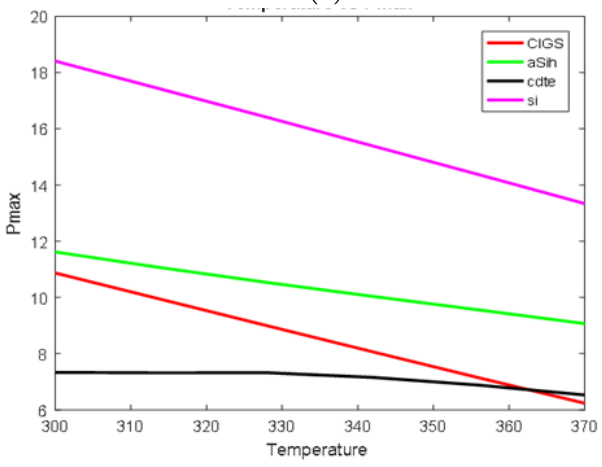

(c)

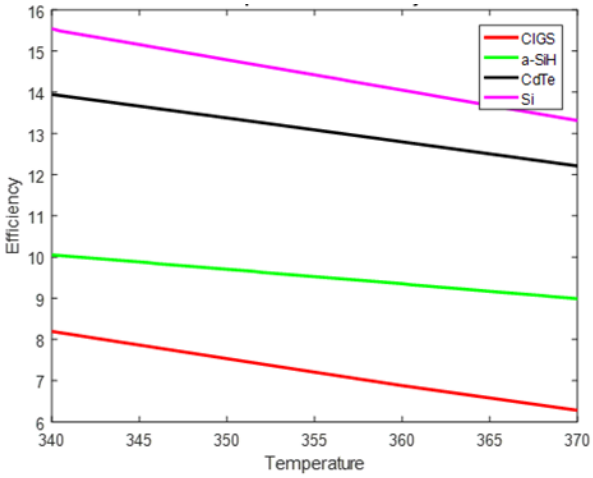

(d)

Figure 7. Variation of different electrical parameters of c-Si, a-Si:H, CdTe and CIGS PV cells with increasing the operating temperature.

Table 6. Temperature coefficient of different IV parameters.

PV cell	$\frac{dv_{oc}}{dT}$ K^{-1}	$\frac{dv_{mpp}}{dT}$ K^{-1}	$\frac{di_{mpp}}{dT}$ K^{-1}	$\frac{dp_{max}}{dT}$ K^{-1}
CIGS	-0.0026	-0.0023	-0.0322	-0.0663
a-Si:H	-0.0028	-0.0024	-0.0016	-0.0362
CdTe	-0.0024	-0.0024	-0.0093	-0.0112
c-Si	-0.0020	-0.0021	-0.0094	-0.0724

Figure 9 shows the quantum efficiency curves of c-Si, a-Si:H, CdTe, and CIGS solar cells individually at room temperature (300K) and high temperature (360K). Quantum efficiency of c-Si solar cell increases as a consequence of high temperature and higher impact has been found in the blue wave region (300-550nm). QE values at 375 nm weres 70.40% and 78% at 300K and 360K temperatures, respectively. The impact of high temperature was significant at low wavelength region (300-550nm) in a-Si solar cell only. The QE characteristics of CIGS at high and low temperature were almost similar and no significant impact has been found. The highest temperature impact on QE has been found in CdTe solar cell throughout the entire wavelength region (300-850nm). This can be the possible reason for the minimum negative temperature coefficient of P_{max} for CdTe solar cell.

https://dx.doi.org/10.46603/ejcee.v1i1.21

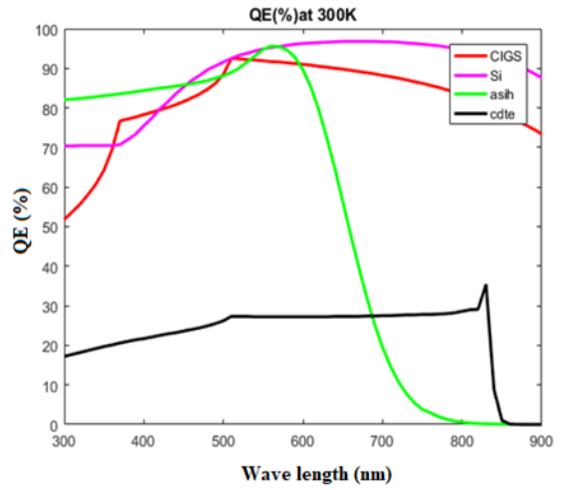

(a)

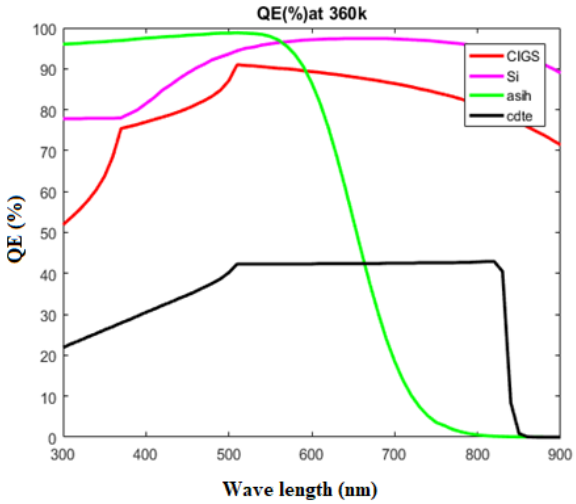

(b)

Figure 8. Comparative quantum efficiency curves of c-Si, a-Si: H, CdTe and CIGS solar cells at 1000W/m2 and (a) 300K and (b) 360K temperatures.

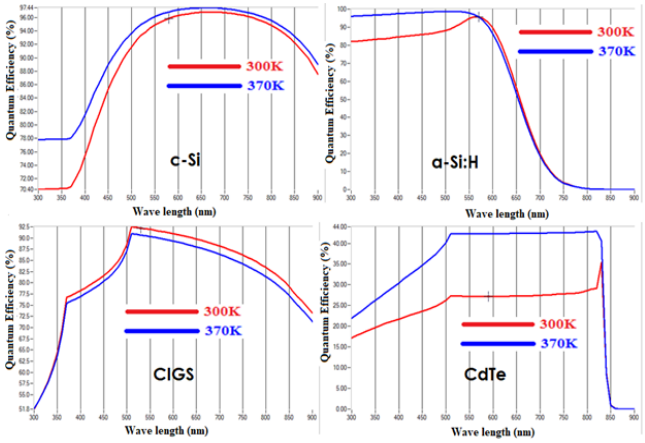

Figure 9. Quantum efficiency curves of c-Si, a-Si:H, CdTe and CIGS solar cells at 1000W/m^2.

4. CONCLUSIONS

Comparative investigations on the effect of operating temperature on the performance of c-Si, a-Si:H, CdTe and CIGS solar cells have been carried out through SCAPS 1D simulation software. Following facts were found as conclusions:

i. The V_{oc}, FF, P_{max}, and efficiency of all four solar cells gradually decrease with the increase of temperature and I_{sc} of all four cells slightly increases with the increase of temperature.
ii. The lowest impact of temperature on Voc was found for the c-Si solar cell with a temperature coefficient of -0.0020/K.
iii. Temperature coefficient values of P_{max} of c-Si, CdTe, CIGS and a-Si were -0.0724/K, -0.0112/K, -0.0663/K, and -0.0362/K, respectively. CdTe solar cell possesses better temperature stability in power generation.
iv. (iv)The c-Si shows better Spectral response comparative to the other three cells, both at high and low temperatures. Quantum efficiency of all four technologies was enhanced at high temperature. The highest enhancement of QE was found in CdTe solar cell.

ACKNOWLEDGEMENT

The authors would like to thank the SCAPS 1D solar cell simulator developers, A. Niemegeers, M. Burgelman, K. Decock & Johan Verschraegen, department of electronics & information system (ELIS), University of Gent, Belgium.

REFERENCES

[1] B. P. Center, "Annual Energy Outlook 2020," 2020.
[2] M. Hosenuzzaman, N. A. Rahim, J. Selvaraj, M. Hasanuzzaman, A. B. M. A. Malek, and A. Nahar, "Global prospects, progress, policies, and environmental impact of solar photovoltaic power generation," Renewable and Sustainable Energy Reviews, vol. 41, pp. 284-297, 2015.
[3] P. G. McCormick and H. Suehrcke, "The effect of intermittent solar radiation on the performance of PV systems," Solar Energy, vol. 171, pp. 667-674, 2018.
[4] K. Kawajiri, T. Oozeki, and Y. Genchi, "Effect of Temperature on PV Potential in the World," Environmental Science & Technology, vol. 45, Issue 20, pp. 9030-9035, 2011.
[5] M. Mani and R. Pillai, "Impact of dust on solar photovoltaic (PV) performance: Research status, challenges and recommendations," Renewable and Sustainable Energy Reviews, vol. 14, Issue 9, pp. 3124-3131, 2010.
[6] W. Javed and B. Guo, "Effect of relative humidity on dust removal performance of electrodynamic dust shield," *Journal of Electrostatics*, vol. 105, p. 103434, 2020/05/01/ 2020.
[7] A. Sohani, M. H. Shahverdian, H. Sayyaadi, and D. A. Garcia, "Impact of absolute and relative humidity on the performance of mono and poly crystalline silicon photovoltaics; applying artificial neural network," Journal of Cleaner Production, vol. 276, p. 123016, 2020.
[8] A. Khodakaram-Tafti and M. Yaghoubi, "Experimental study on the effect of dust deposition on photovoltaic performance at various tilts in semi-arid environment," Sustainable Energy Technologies and Assessments, vol. 42, p. 100822, 2020.
[9] M. A. Islam, M. Hasanuzzaman, and N. A. Rahim, "Design and Analysis of Photovoltaic (PV) Power Plant at Different Locations in Malaysia," IOP Conference Series: Materials Science and Engineering, vol. 358, p. 012019, 2018.
[10] E. Radziemska, "The effect of temperature on the power drop in crystalline silicon solar cells," Renewable Energy, vol. 28, no. 1, pp. 1-12, 2003.

https://dx.doi.org/10.46603/ejcee.v1i1.21

[11] A. R. Gxasheka, E. E. van Dyk, and E. L. Meyer, "Evaluation of performance parameters of PV modules deployed outdoors," Renewable Energy, vol. 30, no. 4, pp. 611-620, 2005.

[12] Y. Hishikawa, T. Doi, M. Higa, K. Yamagoe, H. Ohshima, T. Takenouchi, and M. Yoshita, "Voltage-Dependent Temperature Coefficient of the I–V Curves of Crystalline Silicon Photovoltaic Modules," IEEE Journal of Photovoltaics, vol. 8, no. 1, pp. 48-53, 2018.

[13] P. Singh and N. M. Ravindra, "Temperature dependence of solar cell performance—an analysis," Solar Energy Materials and Solar Cells, vol. 101, pp. 36-45, 2012.

[14] L. I. Nykyruy, R. S. Yavorskyi, Z. R. Zapukhlyak, G. Wisz, and P. Potera, "Evaluation of CdS/CdTe thin film solar cells: SCAPS thickness simulation and analysis of optical properties," Optical Materials, vol. 92, pp. 319-329, 2019.

[15] F. Anwar, S. Afrin, S. S. Satter, R. Mahbub, and S. M. Ullah, "Simulation and performance study of nanowire CdS/CdTe solar cell," Int. J. Renewable Energy Research, vol. 7, no. 2, pp. 885-893, 2017.

[16] P. Chelvanathan, M. I. Hossain, and N. Amin, "Performance analysis of copper–indium–gallium–diselenide (CIGS) solar cells with various buffer layers by SCAPS," Current Applied Physics, vol. 10, no. 3, Supplement, pp. S387-S391, 2010.

[17] M. Burgelman, P. Nollet, and S. Degrave, "Modelling polycrystalline semiconductor solar cells," Thin Solid Films, vol. 361-362, pp. 527-532, 2000.

[18] K. Decock, S. Khelifi, and M. Burgelman, "Modelling multivalent defects in thin film solar cells," Thin Solid Films, vol. 519, Issue 21, pp. 7481-7484, 2011.

[19] M. Burgelman and J. Marlein, "Analysis of graded band gap solar cells with SCAPS," in *Proceedings of the 23rd European Photovoltaic Solar Energy Conference, Valencia*, 2008, pp. 2151-2155.

[20] S. Degrave, M. Burgelman, and P. Nollet, "Modelling of polycrystalline thin film solar cells: new features in scaps version 2.3," *Proceedings of 3rd World Conference on Photovoltaic Energy Conversion*, vol. 1, pp. 487-490: IEEE, *2003*.

[21] S. Dubey, J. N. Sarvaiya, and B. Seshadri, "Temperature Dependent Photovoltaic (PV) Efficiency and Its Effect on PV Production in the World – A Review," Energy Procedia, vol. 33, pp. 311-321, 2013.

[22] S. Ahmed, F. Jannat, M. A. K. Khan, and M. A. Alim, "Numerical development of eco-friendly Cs2TiBr6 based perovskite solar cell with all-inorganic charge transport materials via SCAPS-1D," Optik, vol. 225, p. 165765, 2021.

https://dx.doi.org/10.46603/ejcee.v1i1.21